Image Cover Sheet

CLASSIFICATION	SYSTEM NUMBER 507269
UNCLASSIFIED	

TITLE

SIMULATION OF MICROSTRUCTURES IN LASER CLAD NICKEL ALUMINUM BRONZES

System Number:

Patron Number:

Requester:

Notes:

SIMULATION OF MICROSTRUCTURES IN LASER CLAD NICKEL ALUMINUM BRONZES

C. V. Hyatt[1], J. A. Gianetto[2], J. C. Bennett[3], M. Sahoo[2], M. W. Letts[2], C. Bibby[2]
[1]Defence Research Establishment Atlantic—Dartmouth—Canada;
[2]Materials Technology Laboratory, CANMET—Ottawa—Canada;
[3]Acadia University—Wolfville—Canada.

ABSTRACT

Experiments to assess the usefulness of weld simulation techniques for understanding phase transformations in the laser cladding of nickel aluminum bronzes showed all weld zones could be successfully simulated using a thermomechanical simulator. Insights into phase transformations were shown to be possible by combining metallography with dilatometry.

RÉSUMÉ

Des expériences ont été effectuées pour évaluer l'utilité de techniques de simulation de soudures pour comprendre les transformations de phase dans le revêtement par laser de bronzes d'aluminium. La microstructure du métal déposé, celle obtenue par réchauffement et celle de la zone affectée par la chaleur ont été simulées de façon satisfaisante et les données ont été recueillies par dilatométrie.

INTRODUCTION

Laser welding has many applications for the reclamation, fabrication, and surface engineering of nickel aluminum bronzes (NAB). These applications make use of the novel microstructures which result from the rapid cooling associated with laser welding (1,2). The fine scale of these weld microstructures complicates understanding the processing-structure-property relationships of these materials. This paper examines whether or not a weld simulation technique can be used for developing this understanding. Specifically, a technique which allows the transformations of liquid weld deposit through the high temperature β phase, to the lower temperature martensite, bainite, solid solution (α) and intermetallic phases is investigated (3). This technique is promising because it provides known thermal conditions and facilitates the monitoring of phase transformations by dilatometry. Techniques potentially useful for generating specimens representative of a particular weld zone and large enough for testing purposes were also investigated.

Simulation of Microstructures in Laser Clad Nickel Aluminum Bronzes

MATERIALS AND METHODS

The compositions of the castings and consumables used in this work are shown in Table 1. Casting A was used as a substrate for cladding experiments while casting B was used for the preparation of most specimens for weld simulation. Casting C was useful for understanding dilatometry results, as it was sufficiently low in aluminum that little high temperature β phase formed. For comparison purposes, and also for use as a starting material for the simulation of reheated zones, wire of the composition shown in Table 1, was clad onto alloy A, using the conditions shown in Table 2. Based on work to be published elsewhere (4), cladding on base alloy A, with the wire composition shown in Table 1, produces an as-deposited microstructure which is a mixture of martensitic, bainitic, eutectoid and precipitate phases. The scale and relative proportion of phases depends strongly on heat input. The reheated zone has been shown to consist of martensitic and Widmanstätten α phases. Again the scale depends strongly on heat input. The structure of the reference weldment used in this work is shown, at low magnification, in Fig. 1. The three main zones of interest, as shown on Fig. 1 are, the (base metal) heat affected zone (HAZ), and the as-deposited (AD) and reheated (RH) weld metal zones. Data on microhardnesses are also shown. Figure 2 shows the various regions of the weldment at higher magnification. The harder and softer zones of the as-deposited material are shown in Fig. 2a. Both of these zones consist of a mixture of dark etching martensite which has been shown by electron microscopy to have a 9-R structure with a high density of precipitates and a lighter etching phase which has a similar structure but is thought to have a bainitic origin (5,6). The reheated zone (Fig. 2b) consists of dark etching martensite and light etching Widmanstätten α. At the prior β boundaries of both the as-deposited and reheated materials, a mixture of allotriomorphic α and α plus kappa III eutectoid can be found (5,6).

Table 1. Compositions of coupons and consumables.

Alloy	Designation	Specimen Composition				
		Cu	Al	Ni	Fe	Mn
A	UNS C95800	80.3	8.75	4.8	4.4	1.4
B	UNS C95800	81.9	9.2	4.7	3.4	0.77
C	UNS C95800	80.3	8.8	4.6	6.1	1.2
wire	(ER) CuNiAl	80.8	9.0	4.6	3.9	1.2

Table 2. Laser welding conditions used for the production of the reference clad weld.

Laser Power W	Travel Speed mm/s	Wire Dia mm	Defocus mm	Number of Layers	Shielding Gas	Heat Input J/mm
3300	21	0.25	10.2	1	Argon	150

Simulation experiments were carried out with a Gleeble 2000 simulator. This device allows a bar type specimen to be resistance heated and cooled at rapid and controllable rates (6). By control of heat flow to the jaws that hold the specimen, maximum temperature is reached across a uniform but narrow cross section of the bar. The thermal history of this part of the bar is recorded with a thermocouple spot welded to its surface. Cooling by a variety of means including air and water quenching can be used to produce rapid quench rates. The device allows the radial dilatation of the hot zone to be monitored to track phase transformations. Transformation temperatures can be identified from changes in slope on the dilatation versus temperature plot. Preliminary experiments were carried out on bars cut from the base metal castings to identify transformation temperatures and learn about the behavior of the heat affected zone regions. Experiments were also carried out with a Linses quench dilatometer. This device allows the longitudinal dilatation of specimens about 20 mm long to be measured during quenching at rates as high as 75°C/s.

To simulate the as-deposited material, round bars, 9.84 mm in diameter, were machined from alloy B. The round bars were designed to have a quartz sleeve fit over the sample to contain the melt zone produced by heating their centre to a temperature above the solidus temperature~1040°C. The bars and thermal cycles are shown in Fig. 3a. The bar was rapidly heated so that the hot zone was above 1040°C but below the liquidus temperature~1065°C. The partially melted zone thus produced was rapidly quenched by breaking the glass sleeve immediately after the specimen began to cool and quenching with a water spray system or an air quench. The cooling time, $\Delta t_{800\text{-}500°C}$, for water quenching was 0.4 seconds, corresponding to a cooling rate of 750°C/s. The cooling time $\Delta t_{800\text{-}500°C}$ for air

Simulation of Microstructures in Laser Clad Nickel Aluminum Bronzes

quenching was 1.6 seconds, corresponding to a cooling rate of 188°C/s.

To simulate reheated material, round bars produced by the method just described were machined to a 6 mm diameter in the vicinity of the melt zone and subjected to one reheating cycle to 1000°C followed by a hold at temperature and quenching by water or air. A cooling time $\Delta t_{800\text{-}500°C}$ of 0.1 seconds, corresponding to a quench rate of 3000°C/s was achieved for water quenching. A cooling time $\Delta t_{800\text{-}500°C}$ of 1.6 seconds, corresponding to a quench rate of 188°C/s was achieved for air quenching. A schematic of the thermal cycles used is shown in Fig. 3b. For the air quench case, dilatation measurements were made on the specimen during thermal cycling.

In another experiment to establish the effect of reheating on the microstructure of the weld, specimens (10 x 10 x 70 mm) were machined, as shown in Fig. 3c, from the laser clad weldment. As shown schematically in Fig. 3c, these specimens were heated to 1000°C, held at temperature for 1 second, then water quenched.

RESULTS

Figure 4a shows a representative dilatometric curve obtained with a $\Delta t_{800\text{-}500}$ of ~ 1 s and alloy B. Figure 4b shows the microstructure produced by this thermal cycle. Comparing the microstructure in Fig. 4b with those of the heat affected zone of the clad weld in Figure 1 and other welds (1,3), shows this approach to provide a reasonable simulation of heat affected zone structures. The major points of transformation, corresponding to changes in volume, have been indicated on Fig. 4a. Based on continuous cooling transformation diagrams (7), it is likely that the cooling transformation observed to start at a temperature of ~855°C is the β phase in the high temperature $\alpha+\beta$ structure transforming to α. This probably occurs initially by the growth of the α regions and subsequently by the formation of α with a Widmanstätten morphology. This transformation seems to be complete by 620°C. Some formation of intermetallic kappa phases and perhaps eutectoid may occur in this range as well. The change in slope at 565°C may correspond to the precipitation of κ_{IV}, while the change in slope at 170°C, is probably from a diffusionless martensite transformation. Support for this conclusion comes from quench dilatometry experiments which showed this curvature at 170°C only occurred in alloys like alloy B, but not in alloys like alloy C, in which little martensite forms. These results show that further work is necessary to fully understand the dilatation measurements. They also show that laser weld heat affected zone structures can be simulated and dilatation data can be collected. Work reported elsewhere showed that there is a strong link between the starting microstructure and that which is formed as a result of reheating either in the simulated or in the real heat affected zones (3).

Simulated as-deposited specimens heated to 1040°C and 1064°C and water quench exhibited similar almost fully martensitic microstructures. Figure 5a shows the microstructure of a specimen water quenched from 1040°C. As with the higher hardness part of the reference weld (Fig. 2a), the prior β grains were outlined by a light etching phase, which is probably allotriomorphic α. As well a light etching phase with Widmanstätten morphology, either Widmanstätten α or bainite, was observed to form on the prior β grain boundaries. Again, this is similar to the as-deposited weld metals. Microhardness, in the simulation experiments in which water quenching was used, depended on peak temperature. Specimens heated to 1040°C displayed an average hardness of 331 HV and while those heated to 1064°C had an average hardness of 360 HV. These are within the range of hardnesses measured in the as-deposited zone of the laser weld (Fig. 1). Though the simulated as-deposited microstructures produced by water quenching were in many respects similar to the actual as-deposited material, the prior β grain size was substantially larger. As well, in the simulation specimens the prior β grains were equiaxed rather than columnar, as they were in the actual welds.

Simulated as-deposited material produced by air quenching from 1040°C exhibited a softer ($\leq$ 245 HV) microstructure (Fig. 5). Again, the prior β grains were coarse and allotriomorphic α and some Widmanstätten α were evident at the grain boundaries. Within the grains, there was a dark etching phase interspersed between the α laths. The precise morphology and identification of the phases that make up the dark etching region have not yet been determined, however, the dark etching region is similar to that found in higher heat input welds (3).

Transmission electron microscopy (TEM) was used to further characterize the microstructure of the simulated as-deposited material produced by water quenching from a temperature of 1040°C. The bright-field micrograph of this

Simulation of Microstructures in Laser Clad Nickel Aluminum Bronzes

material in Fig. 6a reveals the presence of two major constituents along with several precipitate phases. Electron diffraction analysis indicates the matrix is composed of inter-dispersed plates of α phase and martensite. At higher magnification, the martensite plates may be seen to be composed of small (< 20 nm in width) domains which are twin-related and based on 9R long-period stacking order (Figs. 6b and 6c). Similar superstructures, which are derived from a fcc subcell via the periodic insertion of stacking faults after every third close-packed layer, have previously been identified in NAB castings and welds (5,6). Stacking faults of this type are also found within the α phase plates and an ordered, 9R structure equivalent to that of the martensitic phase is observed, although in this case the domains are on a much larger scale (Fig. 6d). The increased domain size suggests a different, possibly bainitic, origin for the superstructure in the α plates. In addition, a high density of cuboidal precipitates ranging in size from 10 to 50 nm is observed in both the 9R α (bainitic?) plates and martensitic phase. Energy dispersive x-ray microanalysis indicates that these particles are Fe-rich and presumably related to the κ_{IV} precipitates previously identified in NAB castings (7).

The structural details of the simulated as-deposited material produced by water quenching from 1040°C revealed by electron microscopy are similar to those observed in the as-deposited material in the reference weld. This can be confirmed by comparing Fig. 6e, which shows the structure of the as-deposited material in the reference weld, with Fig. 6a. Figure 6e reveals that the actual as-deposited material also consists of a dual phase matrix of α and martensite plates along with various precipitate phases. The observed morphologies of the matrix phases are comparable to those found in the simulated as-deposited material. A similarly high density of Fe-rich precipitates was detected throughout both phases (Fig. 6e) and the martensite plates were again comprised of small, twin-related domains with 9R crystal structure that are apparently isostructural with those described above (Fig. 6b). There was a minor difference in the crystal structure of the α phase. In the simulated as-deposited material, the α plates adopt the 9R superstructure exclusively (Fig. 6d). However, in the as-deposited weld metal of the reference weld, the 9R structure predominates but variable, and often substantially reduced, stacking fault densities also occur. This is likely a result of a more uniform temperature profile in the simulation experiment. In summary, optical and electron microscopy showed that most features of the as-deposited material can be reproduced by the simulation method. A disadvantage of the simulation method is that it produced a relatively coarse equiaxed prior β grain structure that is substantially different from that found in real welds. However, from the perspective of understanding microstructural development, this should be a minor effect, probably only changing the density of nucleation sites where α phases could form.

The microstructures of specimens intended to simulate reheated material produced by heating to a peak temperature of 1050°C, water quenching, reheating to 1000°C and either air or water quenching, are shown in Figs. 5c and 5d. As with the simulated as-deposited material, the prior β grain sizes are substantially coarser than those of the reference laser weld. The specimen water quenched following reheating to 1000°C had a microhardness between 299 and 400 HV (average 354) while the air quenched specimen had a hardness of HV 227-342 (average 292). The specimen reheated to 1000°C and water quenched, Fig. 5c, resembles the structure produced by partial melting (Fig. 5a) and water quenching, and has a similar microhardness (354 vs. ~360 HV). The only modification of structure seems to be that the needle-like laths (plates) within the grain interiors in the reheated specimen are not as well defined. The structure had a higher volume fraction martensite than the reheated zone of the reference laser weld and was substantially harder. With air quenching a completely different structure (Fig. 5d) and a decrease in microhardness (~360 to 292 HV) were observed. The dilatometric results for this thermal cycle showed that a much larger volume fraction of original martensitic microstructure was transformed on heating at ~700°C. As can be seen in Fig. 5d, the transformed microstructure contained allotriomorphic and Widmanstättan α at the prior β boundaries as well as a Widmanstätten α structure within the grain interiors. Some dark etching martensite was also present. The structure shown in Fig. 5d was similar to, but much coarser, and somewhat harder than that which formed in the reheated zone of the reference weld. It was similar to reheated zone structures observed in gas tungsten arc and gas metal arc welds, but was substantially coarser than the reheated zone of the reference laser weld. Based on these preliminary results, neither of the thermal cycling techniques investigated in this section simulated the reheated material in the reference laser weld adequately. The ability to generate dilatometric traces for the simulated reheating cycle was however useful, and the high cooling rates achieved may be useful for other purposes.

Simulation of Microstructures in Laser Clad Nickel Aluminum Bronzes

Compared with the technique just discussed, reheating of as-deposited weld metal proved a superior means of simulating the actual reheated weld metal. An example of simulated weld metal produced by reheating to 1000°C, holding for 1 second, then water quenching is shown in Fig. 5e. The simulated reheated weld metal is similar to the coarsest part of the reheated zone (area circled on Fig. 2b) of the reference laser weld. Both microstructures consist of grain boundary allotriomorphic α, Widmanstätten α and martensite, with similar prior β grain sizes and shapes. The hardness of the simulated reheated weld metal (HV 203 to 230) was similar to that of the actual reheated weld metal (HV 215-260). Thus this simulation technique offers a reasonable means to generate a simulated reheated zone material which closely approximates that in the actual welds. A volume of such material 1 mm by 10 mm by the depth of the deposit was generated on one specimen in the current study. This is substantially larger and more useable than the 50 μm wide reheated zones seen on the actual specimens. Long term corrosion studies are currently ongoing with such specimens. Data on the effect of peak temperature and time at temperature for simulated reheated material can also be generated with this method (3). This data could allow the start temperature for various transformations to be determined and tempering transformation diagrams and models relevant to the reheating of weld metal to be developed.

DISCUSSION

There are several significant results from this study. First, all zones of relatively low heat input welds can be simulated adequately for many purposes. Second, for the sake of producing homogenous specimens which are much larger than the weld zones they represent, successful techniques have been developed for both heat affected zones and reheated zones under cooling rates representative of laser cladding. The simulation of as-deposited material was also successful except that the prior β grains were of much different size and shape. These larger samples are useful for corrosion experiments. Third, the use of dilatation measurements to obtain phase transformation data has been demonstrated, though with the present equipment and specimen types, such measurements are limited to cooling rates achievable with a free air cool. Correlating this data with the results of transmission electron microscopy, which has been used to identify the phases, provides a basis for understanding the transformations.

Additional work to understand this simulation process and phase transformations in laser clad nickel aluminum bronzes is ongoing. It includes comparison of simulation experiments with welds for which the thermal cycles are known. The collection of dilatometric and metallographic data on nickel aluminum bronzes of different compositions is also being performed. This should allow the origin of various features on the dilatometric traces to be better used and understood. Methods to allow phase transformation data to be collected from high quench rate specimens would be useful.

CONCLUSIONS

Weld simulation techniques have been used to simulate the microstructures of the as-deposited and reheated weld metal and base metal heat affected zones of a nickel aluminum bronze laser weld clad produced with a heat input of 150 J/mm. In general, reasonable agreement between the simulated and actual laser weld microstructures was obtained. Some differences in grain size and shape were noted. The work showed useful phase transformation data can be obtained and specimens large enough for corrosion studies can be generated.

REFERENCES

1. C. V. Hyatt, J. C. Bennett, G. Pelletier, K. KarisAllen, J. Hewitt, J. Gianetto and M. Sahoo, in Proceedings of the 3rd CF/CRAD Meeting on Naval Applications of Materials Technology, edited by J.R. Matthews (DREA, Dartmouth, N.S., 1997) pp. 280-298.
2. C.V. Hyatt, K.H. Magee, J. Hewitt and T. Betancourt, in Proceedings of the 2nd CF/CRAD Meeting on Naval Applications of Materials Technology, edited by J.R. Matthews (DREA, Dartmouth, N.S., 1995) pp. 226-252.
3. J.A.Gianetto, M.Sahoo, M.W. Letts and C.Bibby, The Microstructural Characterization of NiAl Bronze Weldments, DREA CR/95/435, (DREA,, Dartmouth, N. S. 1995).
4. C. V. Hyatt, K.H Magee, and T. Betancourt, Submitted to Metallurgical Transactions, 20 Sept 1997.
5. J.C. Bennett and C.V. Hyatt, proc. Micr. Soc. of Canada, 24, 70-71 (1997).
6. J.C. Bennett and C.V. Hyatt, IBID 1, pp. 321-339.
7. P. Bezina, Int. Metals Reviews, 27, 77-121 (1982).

Simulation of Microstructures in Laser Clad Nickel Aluminum Bronzes

(346-365 HV)   (304-329 HV)   (363-429 HV)
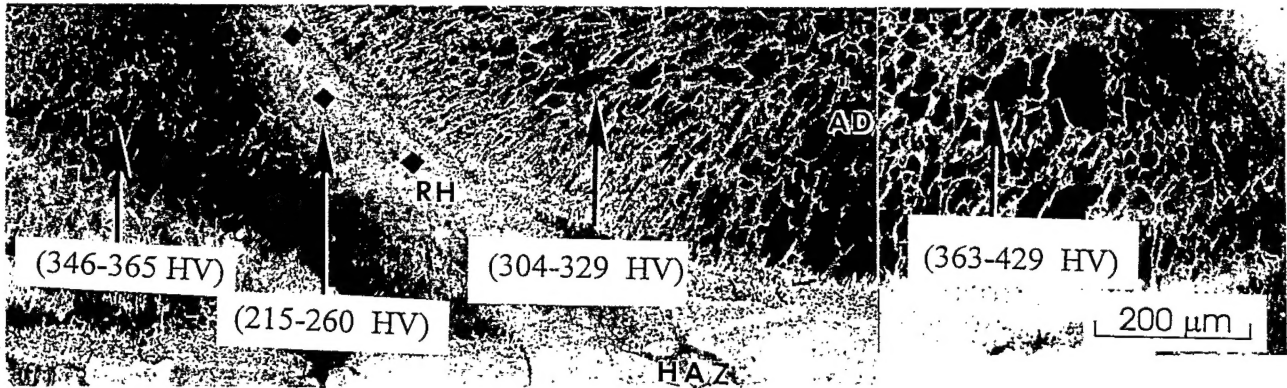
(215-260 HV)   200 µm

RH   AD   HAZ

Figure 1. Low magnification optical micrograph of the reference laser weld. Microstructures of the heat affected zone (HAZ), as-deposited weld metal (AD), and reheated zone (RH) can be seen along with typical microhardness data.
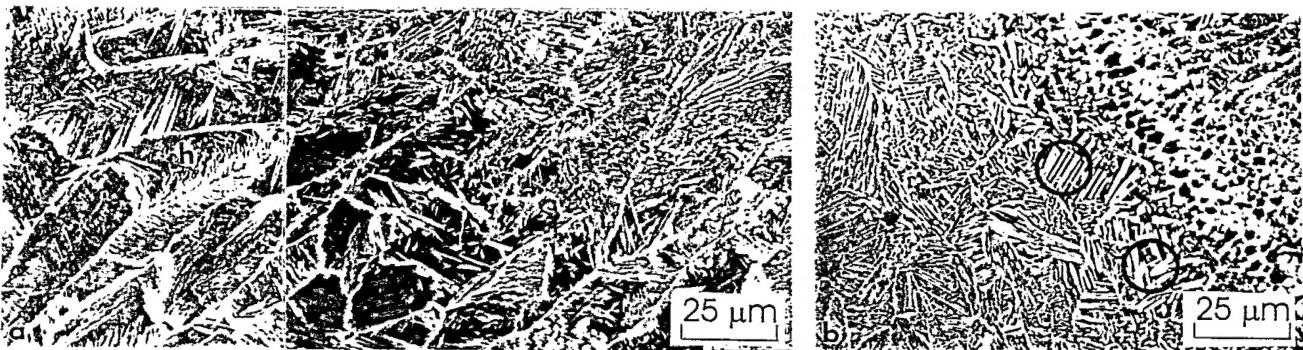

25 µm   25 µm

Figure 2. Micrographs of zones of the clad weldment. a. As-deposited zone, showing hard (h) and soft (s) zones. b. Reheated zone.

$T_{melt} = 1050-1065°C$

20 s hold time

glass sleeve is broken then water quench is applied

Thermocouple   Quartz Sleeve

End-View

(a)

$T_{p2} = 1000°C$ or $800°C$

1 s hold time

air cooled

water quenched

Thermocouple

Radial dilatometer

(b)

$T_p = 1000°C$ and $800°C$

1 s hold time

water quench

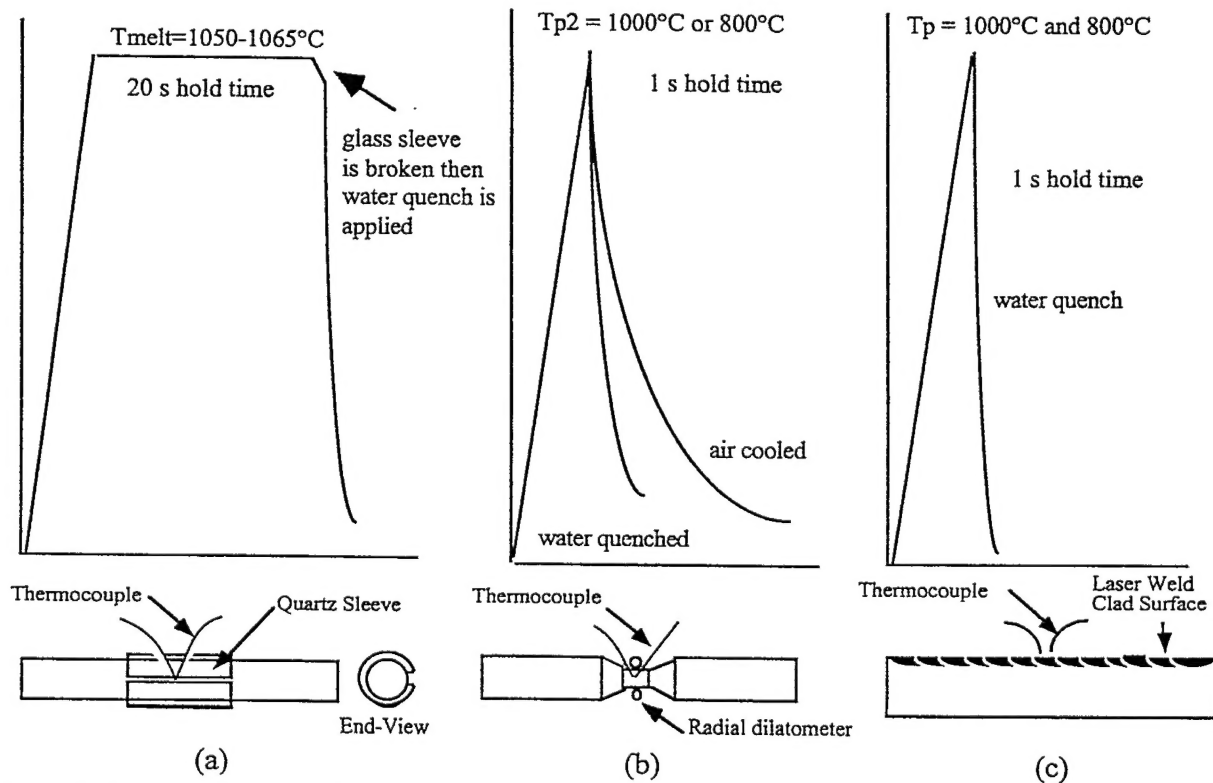Thermocouple   Laser Weld Clad Surface

(c)

Figure 3. Schematic diagrams of the thermal cycles and corresponding Gleeble simulation specimens used in this work. a. Simulated as-deposited material. b, c. Simulated reheated material.

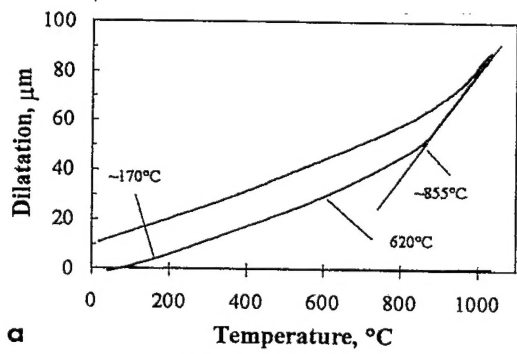# Simulation of Microstructures in Laser Clad Nickel Aluminum Bronzes

Figure 4. Dilatometric curve (a) and microstructure (b) for a simulated heat affected zone in alloy B.
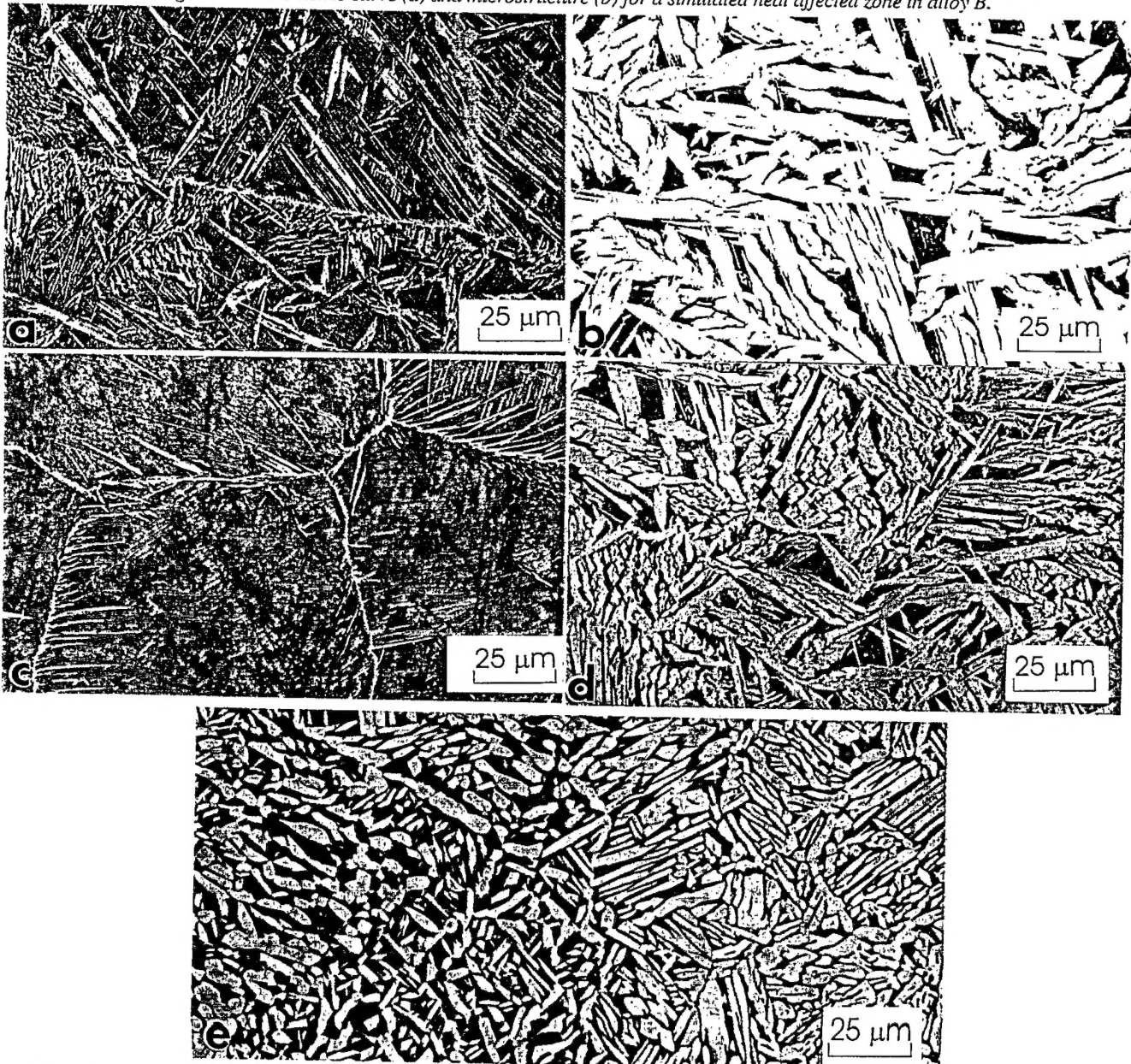

Figure 5. Simulated as-deposited material (a) produced by heating to 1040°C followed by water quenching. (b). Same as (a), but forced air quenching. Simulated as-deposited material produced by heating to 1050°C, water quenching, reheating to 1000°C and either (c) water or (d) air quenching. (e) Laser clad weld metal reheated to 1000°C, held for 1 second, then water quenched.

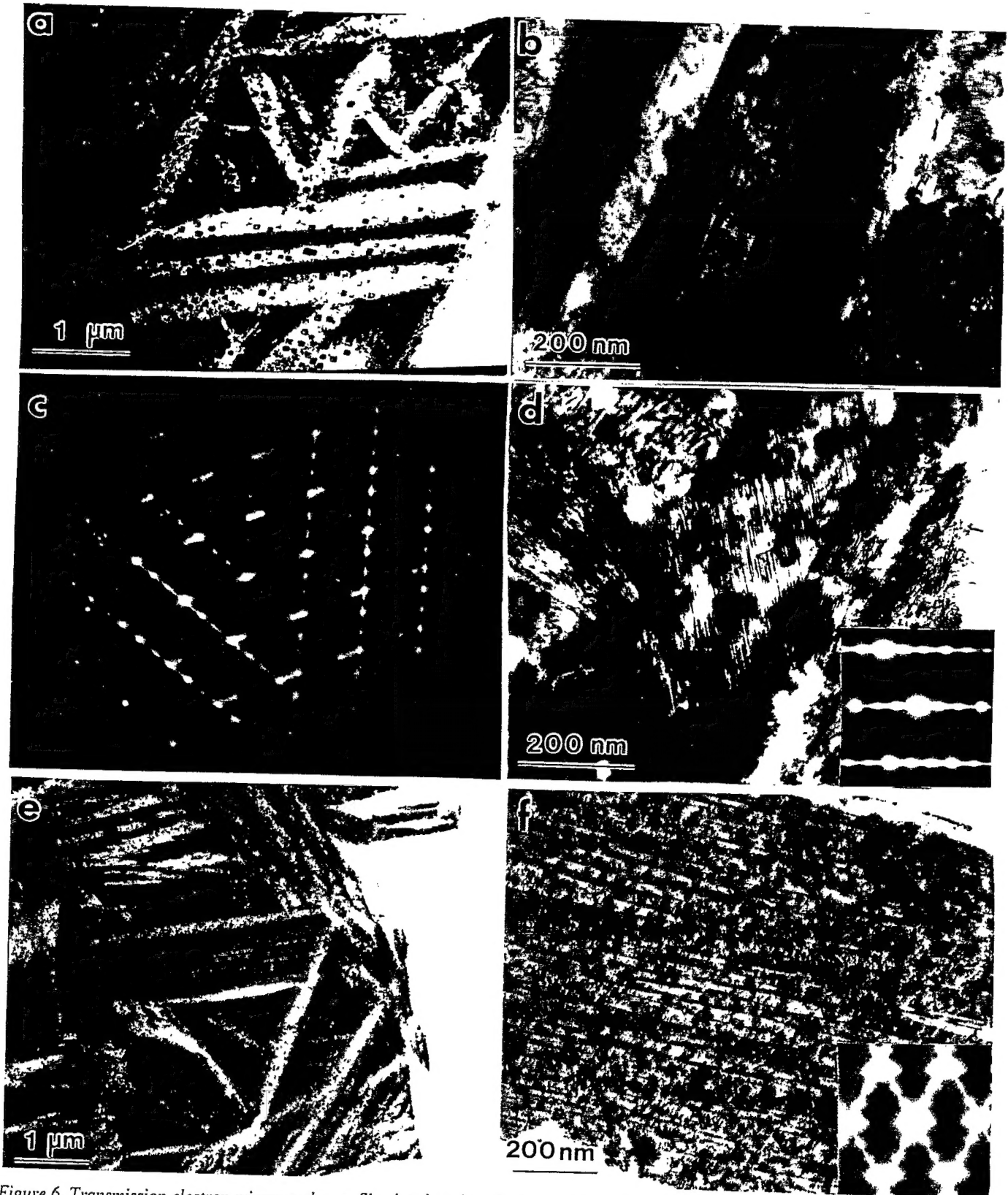# Simulation of Microstructures in Laser Clad Nickel Aluminum Bronzes

Figure 6. Transmission electron micrographs. a. Simulated as-deposited material produced by heating to 1040°C and water quenching. b. Martensite plate in the simulated as-deposited material. c. [110]$_{fcc}$ zone axis selected area electron diffraction pattern (SAEDP) for the martensite plate shown in b. d. 9R α phase plate with stacking faults viewed edge-on (inset - [110] z a. SAEDP). e. As-deposited zone of the reference weld. f. Martensite plate in the reference weld (inset - [110] z a. SAEDP).

507269